catalysts

MDPI

Article

Modified Gasification-Slag-Driven Persulfate Activation for Highly Efficient Degradation of Acetaminophen: N/O Active Site Regulation and Nonradical Oxidation

Wenhao Si [1,2,†], Fei Qi [2,†], Kangjun Wang [1], Qiang Wang [2], Zequan Zeng [2,*], Yuting Niu [2] and Zhanggen Huang [2,3,*]

[1] College of Chemical Engineering, Shenyang University of Chemical Technology, Shenyang 110142, China; 13555855295@163.com (W.S.)
[2] State Key Laboratory of Coal Conversion, Institute of Coal Chemistry, Chinese Academy of Sciences, Taiyuan 030001, China; qifei@sxicc.ac.cn (F.Q.)
[3] University of Chinese Academy of Sciences, Beijing 100049, China
* Correspondence: zengzequan@sxicc.ac.cn (Z.Z.); zghuang@sxicc.ac.cn (Z.H.)
† These authors contributed equally to this work.

Abstract: With the development of coal chemical technology, a large amount of gasification slag and wastewater are produced through coal gasification. Efficient gasification slag utilization and wastewater treatment have attracted much attention. In this study, gasification slag was modified and used as a low-cost and efficient catalyst to activate persulfate for acetaminophen degradation. Via the analysis of high-resolution X-ray photoelectron spectroscopy, the surfaces of nitric acid and calcined modified gasification slag retained a considerable number of carbonyl and graphite N functional groups. These proved to be effective active sites for the activation of persulfate. X-ray diffraction analysis revealed that the gasification slag was composed of carbon and SiO_2. The evaluation of catalytic activity and application of density functional theory proved that the interaction between carbonyl and graphitic nitrogen significantly affected the catalyst activity. When the ratio of graphitic nitrogen to carbonyl was 1:3, the adsorption and activation of persulfate were significantly enhanced. The results of the quenching experiments also confirmed that the non-free radical pathway is the main pathway to activate persulfate using the gasification slag. This study provides a new approach to industrial waste utilization in wastewater treatment.

Keywords: persulfate; gasification slag; nonradical oxidation; acetaminophen

Citation: Si, W.; Qi, F.; Wang, K.; Wang, Q.; Zeng, Z.; Niu, Y.; Huang, Z. Modified Gasification-Slag-Driven Persulfate Activation for Highly Efficient Degradation of Acetaminophen: N/O Active Site Regulation and Nonradical Oxidation. *Catalysts* **2023**, *13*, 1512. https://doi.org/10.3390/catal13121512

Academic Editors: Albin Pintar and Gregor Žerjav

Received: 6 October 2023
Revised: 28 November 2023
Accepted: 5 December 2023
Published: 15 December 2023

1. Introduction

It is well known that acetaminophen (APAP) is a pharmaceutical compound used extensively as an analgesic and antipyretic drug and is one of the most commonly detected pharmaceutical compounds in aquatic environments [1,2]. APAP is also an emerging environmental endocrine disruptor that is likely to pose a threat to the environment and human health [3,4]. APAP is difficult to remove using traditional bio-treatment processes due to its stable chemical structure [5,6].

Persulfate-based advanced oxidation technology (PS-AOP) has been widely considered an effective method for pharmaceutical wastewater treatment because of its high oxidation potential, wide pH range, and long half-life of sulfate radicals [7,8]. Several approaches, such as catalysts (transition metal ions, metal oxides, and carbon), ultraviolet (UV), and ultrasonic (US) methods, have been proposed to activate persulfate for the formation of oxidative active species [9]. Carbon catalysts are effective for persulfate activation with no secondary metal leaching and have been widely investigated [10].

Carbonyl and graphitic N functional groups are the key sites to activate persulfate for the treatment of tetracycline (TC), and 90% degradation is achieved in 20 min at 25 °C [11,12]. However, the high cost and radical interference caused by water impurities

have hindered the application of PS-AOPs with carbon catalysts. To conquer these limitations, a cheap carbon catalyst was prepared with urea as the raw material and used to activate persulfate for cost reduction [13]. Nitrogen doping can also regulate the persulfate activation path to obtain nonradical active species with an anti-interference property [14]. Xu et al. [15] proposed a 3D N-doped porous carbon to activate peroxymonosulfate via a nonradical pathway to oxidize chlorophenols from wastewater. However, carbon catalysts with large specific surface areas and high activities are still expensive [16], and the regulation mechanism of the PS activation path is still unclear.

Coal gasification slag (CGS) is a mixture of residual carbon produced by the coal gasification process [17], with a high carbon and nitrogen content, well-developed porous structure, low price, and wide application [18–20]. It has been proven that modified CGS is an effective and inexpensive catalyst for pollutant removal [21,22]. Liu et al. [23] prepared a microsphere material for the adsorption of Pb (II) and Congo red by combining fine CGS with silica. Fe-doped CGS has been successfully used to activate PMS for the removal of sulfamethoxazole [22]. As a metal-free and high-efficiency carbon catalyst, the performance of persulfate activation via CGS for pharmaceutical wastewater degradation has not been evaluated.

As CGS has a variety of nitrogen-containing functional groups and the proportion of nitrogen–oxygen functional groups in CGS is not low, the mechanism of the nitrogen–oxygen functional groups in CGS is still unclear. Thus, the effect of nitrogen and oxygen functional groups on the activation mechanism needs to be further studied to treat complex wastewater.

In this study, nitric acid treatment combined with calcination in nitrogen was used to modify the nitrogen and oxygen functional groups of the CGS. The surface of the active sites was regulated by calcination, and the mechanism of the catalytic activation of persulfate was further regulated to clarify the internal relationship between heteroatom doping and the activation mechanism. The regulatory mechanism of radical oxidation and the nonradical oxidation pathway via heteroatom doping modification was further clarified.

2. Results and Discussion

2.1. Materials Characterization

Through the XRD patterns of the CGS, CGSO, and CGSO300 (Figure 1), it was found that the main peaks of the gasification slag were at 26.603°, 42.464°, and 47.305°. These peaks are ascribed to carbon, indicating that carbon is the main component of gasification slag. The peaks at 20.859°, 36.543°, 38.852°, and 66.546° are ascribed to SiO_2; this shows that the gasification slag comprises some ash, such as SiO_2.

The CGS and modified gasification slag (CGSO and CGSO300) were characterized through BET. It can be seen from Table 1 that the specific surface area and pore volume of the CGS increased after treatment with nitric acid, which is most probably owing to the removal of ash to form new pore channels. The increase in the specific surface areas facilitates the adsorption of pollutants on the CGS. After calcination, some volatile surface oxygen-containing functional groups were decomposed or reacted with charcoal, resulting in the collapse of the pore channels, leading to a decline in the specific surface area and pore volume of CGSO300.

Table 1. BET data of modified CGS.

Samples	S_{BET} (m^2g^{-1})	V_p (cm^3g^{-1})	Pore Size (nm)
CGS	200	0.22	4.3
CGSO	360	0.32	3.6
CGSO300	208	0.21	3.9

As shown in Figure 2a, absorption and desorption experiments were conducted on CGS, CGSO, and CGSO300. The figure shows that their adsorption type is type IV

isothermal adsorption, and the pore structure of the catalysts mainly comprises mesoporous and microporous structures. CGSO300 has a larger micropore proportion, more micropores, and contributes a more specific surface area, which is more conducive to the reaction. This is also confirmed by the aperture size distribution curve (Figure 2b). The mesoporous and microporous structure of the catalyst is conducive to the transport and activation of persulfate for the degradation of APAP.

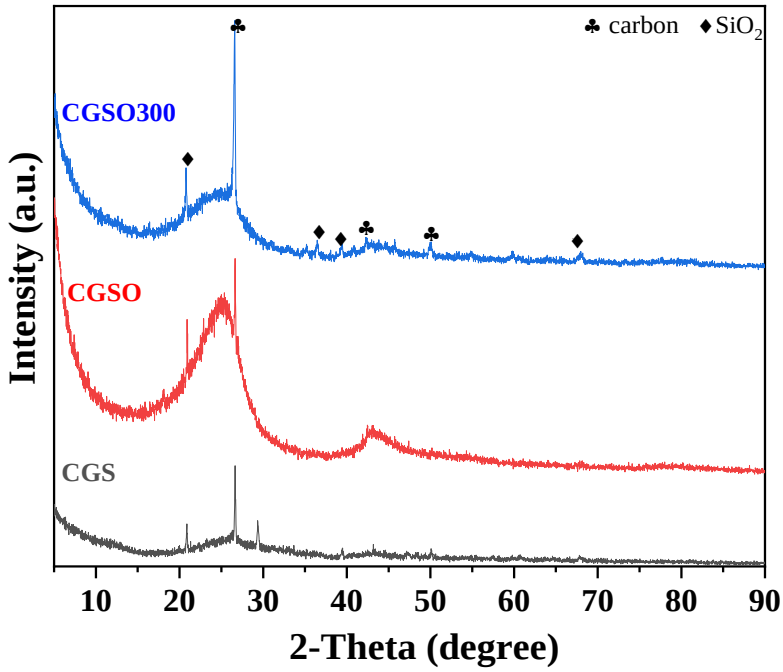

Figure 1. XRD patterns of modified gasification slag.

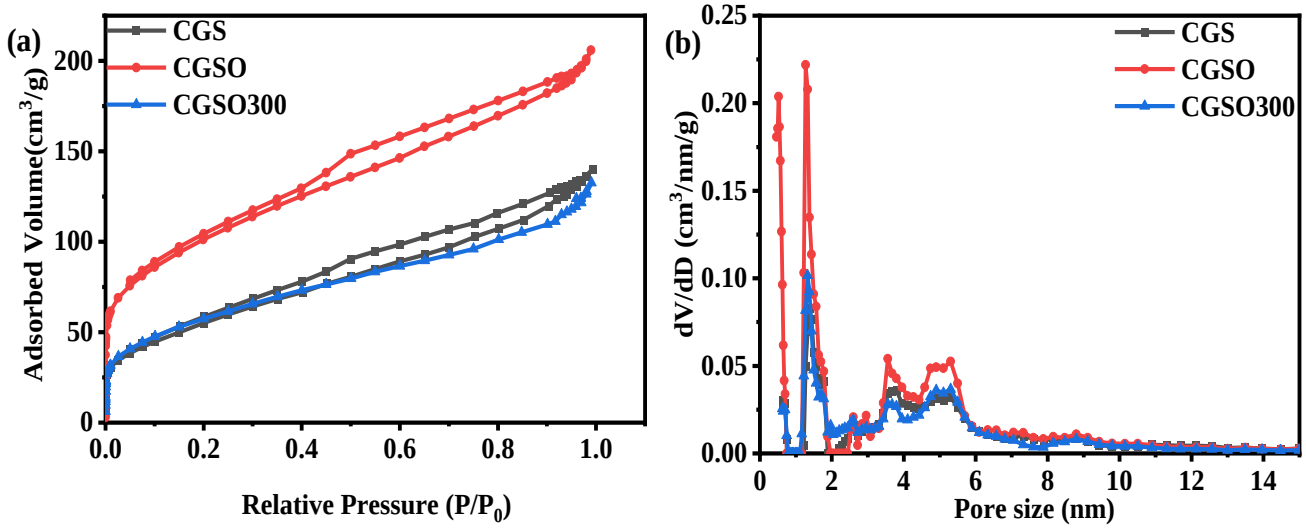

Figure 2. (**a**) N_2 sorption isotherms and (**b**) pore size distribution of modified CGS.

Raman spectra can show the degree of crystallization of a material, reflecting the defects as well as the disorder of the material [24]. As seen in Figure 3, the characteristic D and G bands appear at 1350 cm^{-1} and 1580 cm^{-1}, respectively. The G band represents the in-plane tensile vibration of sp^2 hybrid carbon, which is ascribed to the graphitic properties and reveals the structure of sp^2-bonded carbon. The D band is a disorder-induced vibrational mode ascribed to the fundamental structural defects in the amorphous carbon material. Furthermore, the degree of graphitization and disorder in the carbon

structure is assessed based on the relative intensity ratio of the D spectral band to the G spectral band (I_D/I_G) [25]. It can be seen in Figure 3 that the I_D/I_G values of CGS, CGSO, and CGSO300 are 1.13, 1.20, and 1.29, respectively. Among them, CGS has the highest degree of graphitization, while CGSO300 has the lowest degree of graphitization, which indicates that the crystal structure of CGSO300 is more disordered. A considerable number of oxygen-containing functional groups were formed through nitric acid treatment on the surface of the gasification slag. Further calcination resulted in the decomposition of oxygen-containing functional groups to form a considerable number of defect sites, increasing the disordering of the carbon materials. Demiral et al. [26] found that with the nitric acid modification on activated carbon, the number of carboxyl groups, lactones, and phenyl groups on the surface of activated carbon significantly increased, which increased the disorder of the activated carbon. He et al. [27] found that the modification of graphite with HNO_3 can introduce more defect sites and oxygen/nitrogen-containing groups on graphite. The reason for this is probably the decomposition of the oxygen-containing functional group providing more active sites. More defect sites are conducive to the adsorption and activation of PS.

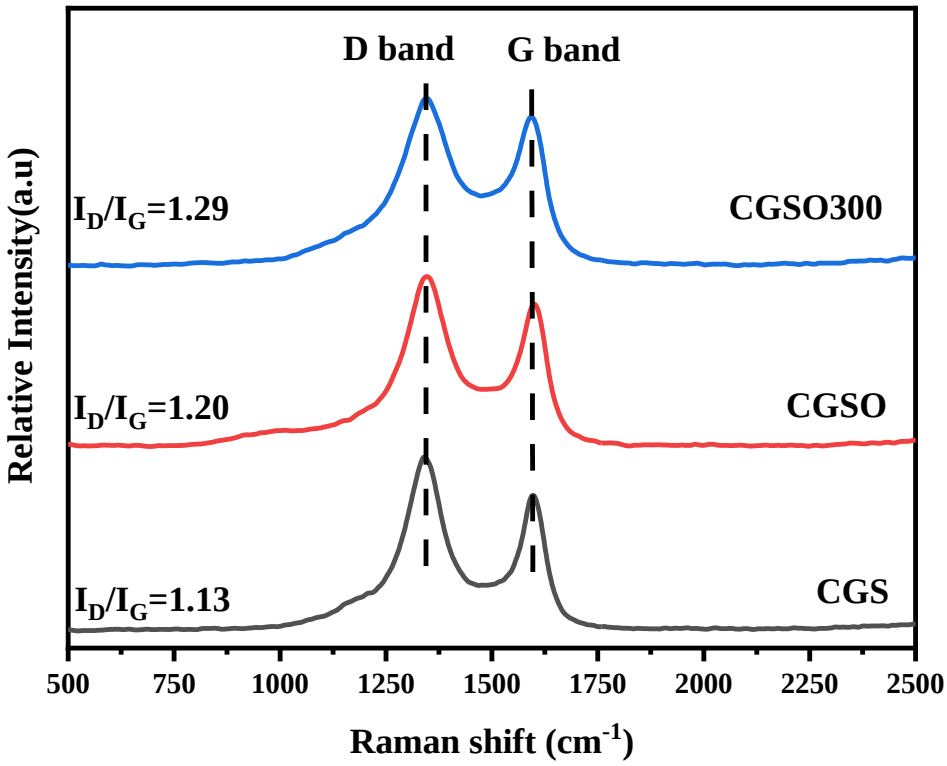

Figure 3. Raman spectrogram of the modified gasification slag.

The modified gasification slags were also characterized using XPS to determine the surface chemical composition and functional group species. Figure 4 shows the XPS broad-sweep curve profile of the modified gasification slags, in which the peaks with binding energies of 284.5 eV, 400.9 eV, and 532.5 eV were ascribed to the elements of carbon, nitrogen, and oxygen, respectively. The atomic concentration of the elements in Table 2 is given through XPS analysis. Since the atomic concentration of elements is obtained using the normalization method, the relative atomic ratio can better reflect the change in element distribution than atomic concentration. It can be observed from Table 2 that, after calcination, both the C/N ratio and O/N ratio significantly decreased. This is because the oxygen-containing surface functional groups formed by nitric acid treatment (CGSO) contain a considerable number of unstable functional groups such as carboxyl groups, which are released in the form of CO_2 and other products during calcination, thus reducing the C and O ratio on the surface. However, the nitrogen-containing functional groups in CGSO

are formed during the formation of gasification slag at high temperatures (800–1400 °C), which has high stability during calcination at 300 °C. So, the relative concentration of the N element increased and the relative concentration of C and O decreased. The other reason is presumably the oxidation of CGS by nitric acid. Compared with the CGS, the oxygen content of CGSO and CGSO300 was substantially enhanced, indicating that a considerable number of oxygen-containing functional groups were successfully formed on the surface of the carbon material [28–30]. The reduction in elemental C and O in CGSO300 compared to CGSO is probably due to the decomposition of the oxygen-containing functional group to CO_2, CO, and H_2O during the calcination process, which indirectly leads to the increase in elemental N content in the modified gasification slag.

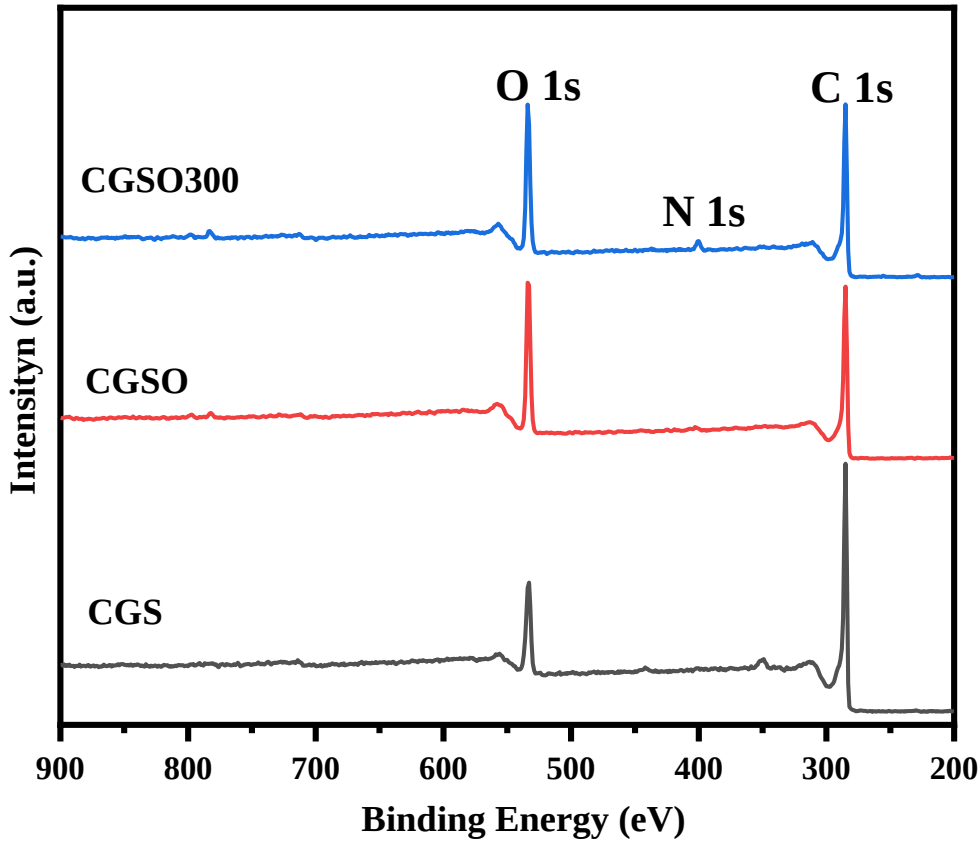

Figure 4. XPS wide-scan profile of modified gasification slag.

Table 2. Surface element composition of modified gasification slag.

Samples	C (at.%)	O (at.%)	N (at.%)	C/N Ratio	O/N Ratio
CGS	82.59	16.27	1.14	72	14
CGSO	71.84	26.71	1.45	49	18
CGSO300	70.15	26.50	3.35	20	7

Figure 5a and Table 3 show the N 1s spectra and the corresponding peak-splitting results. The N 1s spectra can be fitted by four peaks: the peak at 398.5 eV, 400 eV, 401.5 eV, and 404.5 eV are ascribed to pyridine N, pyrrole N, graphitic N, and nitrogen oxides, respectively [31]. On the one hand, the results showed that the proportions of pyridine N, pyrrole N, and nitrogen oxide increased after the modification of CGS with nitric acid due to its strong oxidizing properties. On the other hand, the calcination of CGSO leads to increasing graphitic N owing to the decomposition of pyrrole N and nitrogen oxide.

As shown in Figure 5b and Table 4, it can be seen that the O 1s spectrum can be fitted by five peaks: the peak of 531.1 eV is ascribed to C=O in carbonyl and quinone

groups; the peak of 532.2 eV is ascribed to C=O in anhydride and ester groups; the peak of 533.3 eV is ascribed to C–O in phenol, anhydride, and ester groups; the peak of 535.1 eV is ascribed to oxygen in the form of –COOH; and the peak of 537 eV is ascribed to water in the adsorbed state and CO_2 [32–35]. It is found that the C–O functional group content increases significantly after modification with nitric acid. The carbonyl group content decreased after the CGS was modified by nitric acid to form CGSO and increased after heat treatment to form CGSO300. Carbonyl is a potential active site for PS activation. The loss of carbonyl may lead to a decrease in the catalytic activity of CGSO.

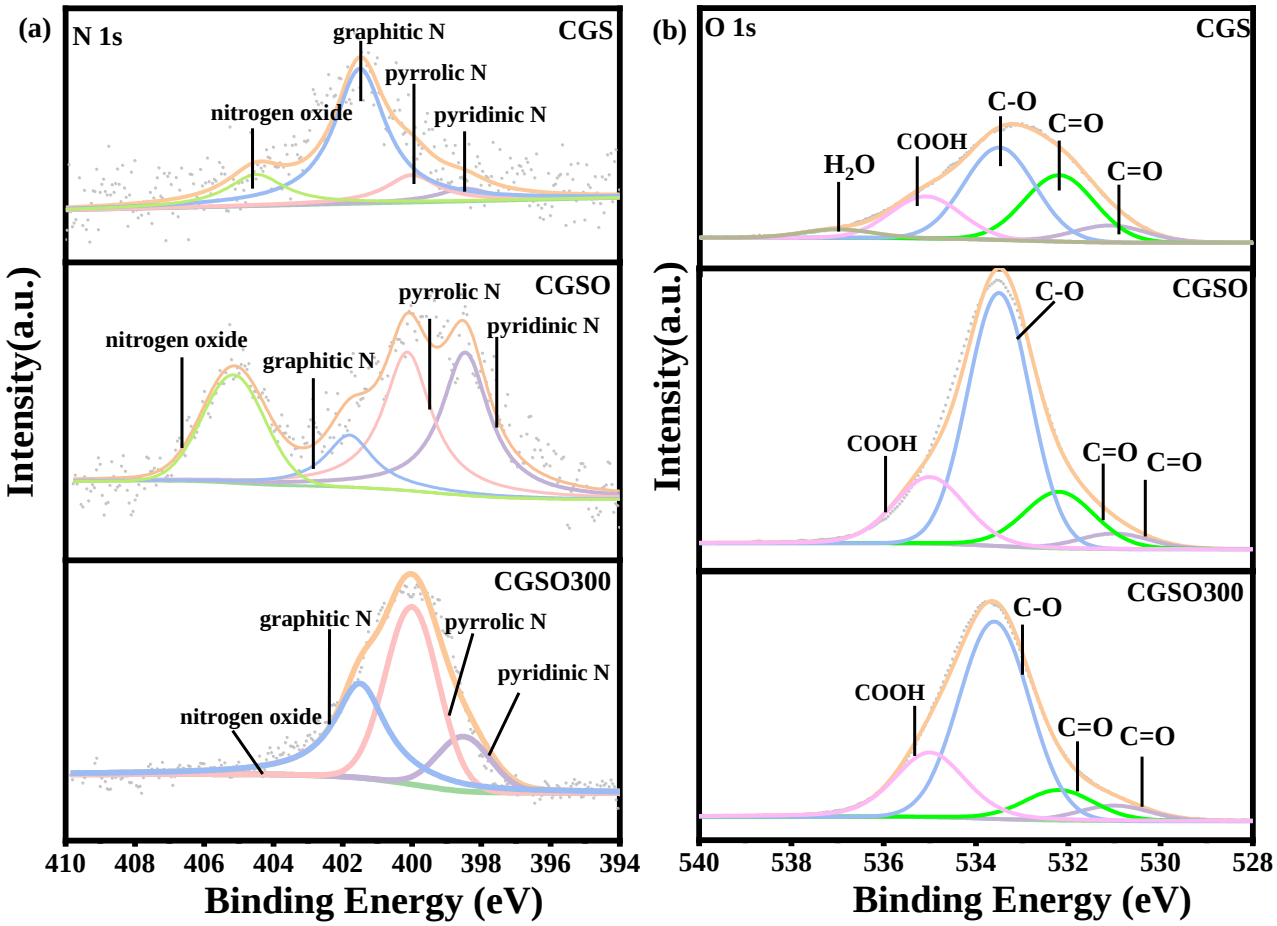

Figure 5. (**a**) N 1s and (**b**) O 1s spectra of modified gasification slag.

Table 3. Nitrogen-containing functional group proportion of modified gasification slag.

Samples	Pyridine N (at.%)	Pyrrole N (at.%)	Graphitic N (at.%)	Nitrogen Oxide (at.%)
CGS	0.07	0.01	0.73	0.19
CGSO	0.48	0.47	0.17	0.32
CGSO300	0.49	0.24	1.26	0.08

Table 4. Oxygen functional group content of modified gasification slag.

Samples	C=O (Carbonyl) (at.%)	C=O (Ester, Anhydride) (at.%)	C–O (Ester, Anhydride, Phenol) (at.%)	COOH (at.%)
CGS	1.3	4.8	6.6	3.0
CGSO	1.1	4.3	16.2	5.1
CGSO300	1.3	2.7	16.4	6.1

2.2. Catalytic Activity for PS Activation

The catalytic activity was evaluated by examining the efficiency of PS activation for the degradation of acetaminophen (APAP), as shown in Figure 6. The insert in Figure 6a shows the adsorption curve of APAP on the modified gasification slag and in the CGS/PS system. APAP could be completely degraded in 40 min with a kinetic rate constant of 0.086 min^{-1}, indicating that the pristine CGS could also activate PS. After the CGSO, the APAP was not completely removed within 50 min with the kinetic rate constant of 0.033 min^{-1}. The reason for this may be the loss of carbonyl, which is an effective site for PS activation. This also may be because the introduction of a considerable number of acidic oxygen-containing functional groups is detrimental to the transfer of electrons from the catalyst to the peroxy-bonds in PS, which greatly inhibits the activation of PS. After calcination at 300 °C, the activation activity of CGSO300 greatly increased with the highest kinetic rate constant of 0.148 min^{-1}. As the nitrogen content of CGSO300 was increased to 6.1% with graphitic N as the dominant nitrogen-containing functional group, the positive charge density of the neighboring oxygen atoms was increased by graphitic N and more readily interacted with PS to form reactive complexes, which enhanced the oxidation of pollutants via the electron transfer pathway.

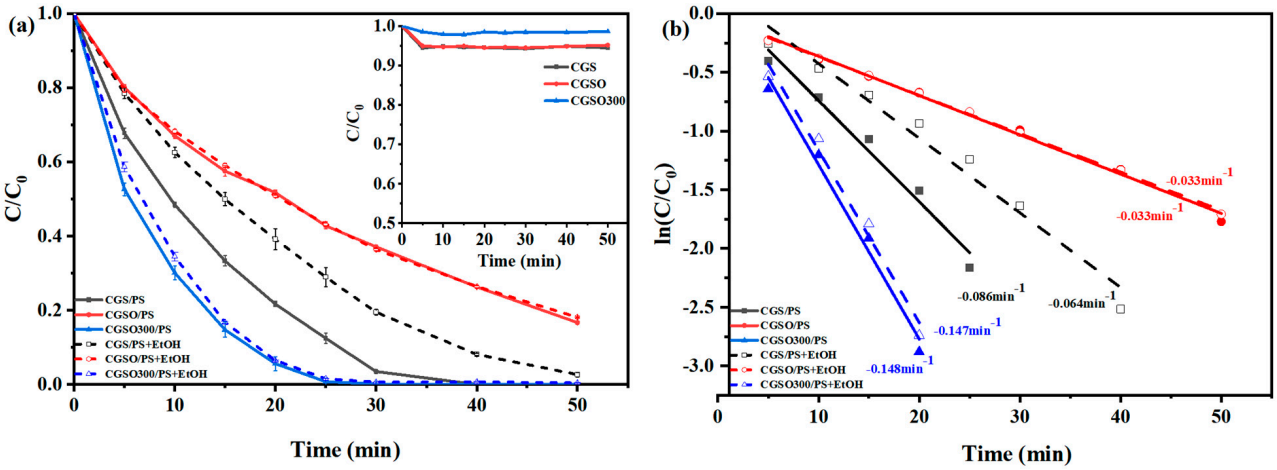

Figure 6. (**a**) Oxidation and adsorption curves and (**b**) kinetic rate of APAP with and without quenching ((APAP) = 50 mgL^{-1}, (CGS) = 0.1 gL^{-1}, (PS) = 2.5 mM, (EtOH/(PS) = 1000).

Ethanol (EtOH) is often used as a trapping agent to quench radicals. Because EtOH had a high reaction rate with both ·OH ($k_{Ethanol/OH} = (1.2 - 2.8) \times 10^9\ M^{-1}s^{-1}$) and $SO_4^{\bullet -}$ ($k_{Ethanol/SO4-} = (1.6 - 7.8) \times 10^7\ M^{-1}s^{-1}$), the reaction rates of CGSO/PS and CGSO300/PS systems were almost unaffected after ethanol was added. This indicated that there are few radicals in CGSO/PS and CGSO300/PS systems and that PS was activated through nonradical pathways. The APAP degradation was inhibited by EtOH in the CGS/PS system with the decreasing kinetic rate constant of 0.086 min^{-1} to 0.064 min^{-1}. Based on Equations (1) and (2), the contributions of nonradical pathways on APAP degradation in CGS/PS, CGSO/PS, and CGSO300/PS systems were calculated as 74%, 99%, and 100%, respectively. It can be found that the nonradical pathway was the dominant activation pathway of PS with modified gasification slag as the catalyst, which benefits the APAP degradation in high-salt wastewater.

$$R_{nonradical} = \frac{k_{nonradical}}{k_{APAP}} \times 100\% \quad (1)$$

$$R_{radical} = 100\% - R_{nonradical} \quad (2)$$

where k_{APAP} and $k_{nonradical}$ represent the total reaction rate constant of APAP oxidation degradation and the rate constant of nonradical oxidation reaction (min^{-1}), respectively.

$R_{radical}$ and $R_{nonradical}$ are the ratios of the radical reaction and the nonradical reaction, respectively.

As is well known, carbonyl and graphitic N are the active sites of carbon materials for persulfate activation, and the ratio of carbonyl and graphitic N can better reflect the catalytic performance of the catalyst. As shown in Figure 7, the reaction activity of the modified gasification slag increased gradually with the increase in the graphitic N and carbonyl content. The coefficient of determinations of graphitic N and carbonyl groups with the reaction rate constant are 0.978 and 0.875, respectively (Figure 7). This indicates that graphitic N and the carbonyl group have an obvious linear relationship with K, and the linear relationship between graphitic N and K is more obvious. The R^2 in Figure 7 is the coefficient of determination of the linear relationship between graphite N, carbonyl, and the kinetic rate constant. The higher R^2 of graphite N indicates that graphite N has a more significant linear relationship with the constant kinetic rate. This may reflect that graphite N has a more significant effect on the catalytic activity. It is indicated that graphitic N may be the main activated site for modified gasification slag due to its higher coefficient of determination.

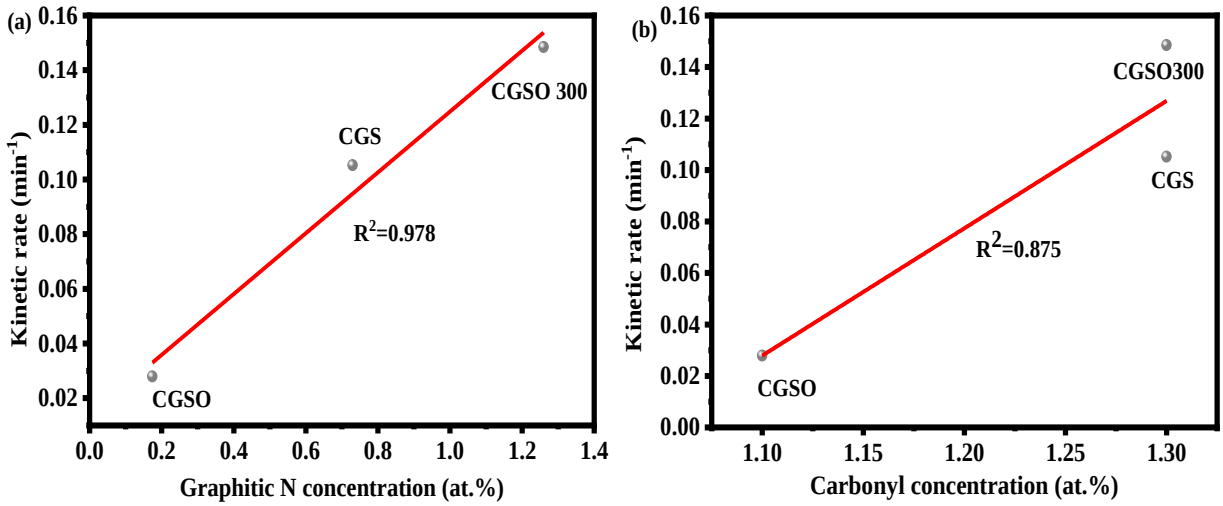

Figure 7. (**a**) Correlation between the kinetic rate and the graphitic N content and (**b**) the correlation between the kinetic rate and the carbonyl content ((APAP) = 50 mgL^{-1}, (CGS) = 0.1 gL^{-1}, (PS) = 2.5 mM).

To reflect the intrinsic activity of the modified gasification slag, the turnover frequency (TOF) values were calculated using Equation (3). As graphitic N and carbonyl are the activity sites, the ratio of graphitic N to the carbonyl group was related to TOF (Figure 8). It can be observed that the ratio of graphitic N to the carbonyl group and TOF has a linear correlation, with a coefficient of determination of 0.921. This shows that graphitic N and carbonyl work together in the activation of PS. As the ratio of graphitic N to carbonyl group increased, the site activity (TOF) increased significantly. This suggests that the graphitic group has a significant influence on the activity of active sites, and the presence of the graphitic group near the carbonyl group is favorable to enhancing the activity of the modified gasification slag.

$$TOF = \frac{k}{(\text{Graphitic N} + \text{Carbonyl}) \times S_{BET}} \quad (3)$$

where TOF is the APAP turnover frequency (min^{-1}gm^{-2}) normalized by carbonyl and graphitic N sites, and k represents the apparent rate constant (min^{-1}). Graphitic represents the atomic ratio of graphitic N. Carbonyl represents the atomic ratio of carbonyl. S_{BET} is the total specific surface area (m^{2}g^{-1}) obtained by the BET test.

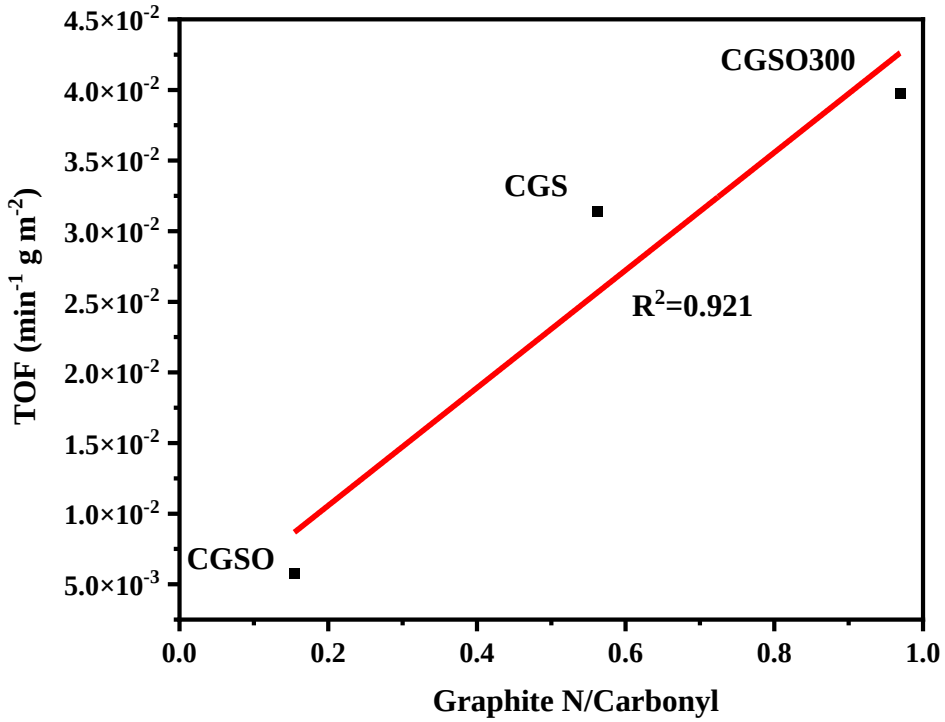

Figure 8. Relationship between the ratio of graphitic N to the carbonyl group and TOF.

2.3. Tests of Catalyst Reusability

To evaluate the reusability of the catalyst for the sustainable operation of the CGSO300/PS system, the catalyst was repeated at room temperature. As shown in Figure 9, the experimental data showed that the catalytic activity of CGSO300 decreased after use. This may be due to the inactivity of the active site on the surface of CGSO300 by oxidation. After calcination and regeneration at 300 °C (after the Used CGSO300 was placed in a tube furnace and heated to 300 °C at 5 °C per minute under a N_2 atmosphere), the activity of CGSO300 was improved, which may be due to the increased active sites such as graphitic N. The states of the N elements in CGSO300 were analyzed (Figure 10 and Table 5), which revealed that the proportion of graphitic N and pyridinic N functional groups on the surface of the Used CGSO300 decreased significantly after use, which may be due to their oxidation by persulfate to form electron-deficient nitrogen oxide functional groups. This makes it difficult for persulfate to continue to activate on its surface, resulting in a significant decrease in catalytic activity. After regeneration at 300 °C, the content of graphitic N functional groups increased, and the catalytic activity partially increased. However, due to the difficulty of converting pyrrole functional groups to active graphite N functional groups at 300 °C, the full recovery of activity may require a higher regeneration temperature. The study found that the content of graphite N decreased and nitrogen oxide increased in CGSO300 after calcination and recovery.

Table 5. Nitrogen-containing functional group proportion of fresh CGSO300 used CGSO300 and regenerated CGSO300.

Samples	Pyridine N (at.%)	Pyrrole N (at.%)	Graphitic N (at.%)	Nitrogen Oxide (at.%)
Fresh CGSO300	0.49	0.24	12.6	0.08
Used CGSO300	0.11	0.25	0.78	1.57
Regenerated CGSO300	0.17	0.28	0.94	1.93

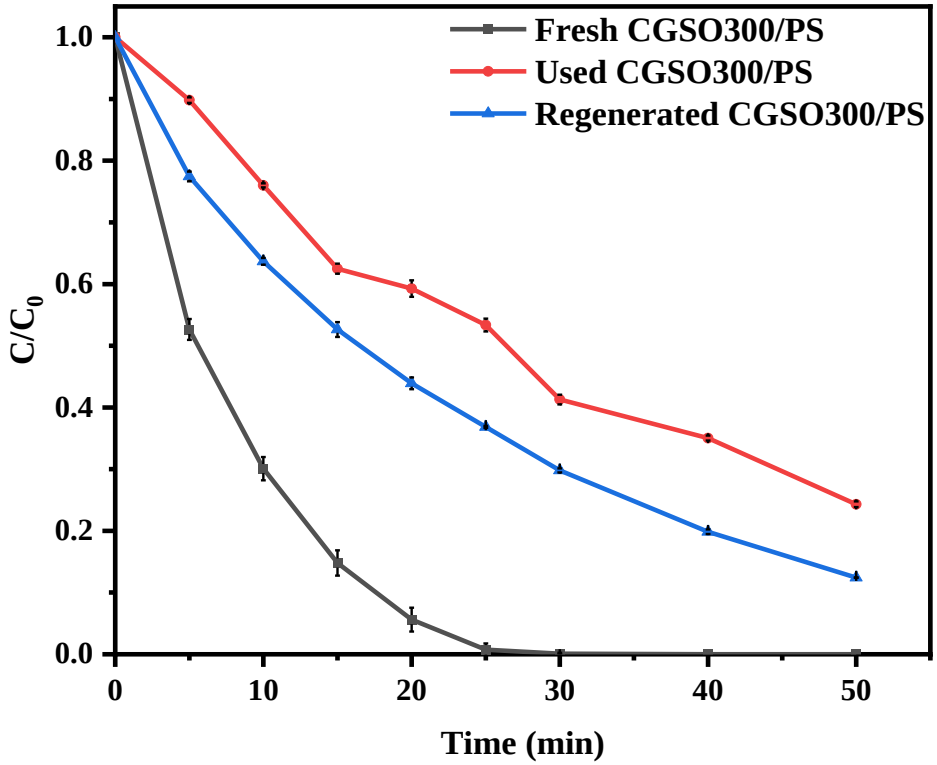

Figure 9. Fresh CGSO300, Used CGSO300, and Regenerated CGSO300 oxidative degradation curves of APAP ((APAP) = 50 mgL^{-1}, (CGSO300) = 0.1 gL^{-1}, (PS) = 2.5 mM).

As shown in Table 6, comparing the data from APAP degradation using different catalytic PS activation approaches shows that biochar has the best catalytic effect on activated PS, with the shortest degradation time and the highest degradation rate. The metal catalyst has a higher preparation cost, longer degradation time, and lower degradation rate.

Table 6. Comparison between CGSO300 and the previously reported different catalysts that activated PS to degrade APAP [36–41].

Catalyst Dosage (gL^{-1})	PS (mM)	APAP (mgL^{-1})	Removal Rate (%)	Pseudo First-Order Kinetics (min^{-1})	References
CGSO300 (0.1)	2.5	50.0	100.0 (25 min)	0.148	This study
Biochar (0.1)	0.5	50.0	100.0 (15 min)	\	[36]
Fe, Cu@g-C_3N_4 (0.01)	1.0	4.0	100.0 (40 min)	0.069	[37]
3DOMFeCo (0.2)	2.0	10.0	100.0 (60 min)	\	[38]
$CuFe_2O_4$ (0.3)	3.4	100.0	91.0 (60 min)	\	[39]
Fe^0 (2.0)	2.0	30.0	98.5 (35 min)	0.129	[40]
Fe_3O_4 (0.8)	0.2	10.0	75.0 (120 min)	0.012	[41]

2.4. Theoretical Calculation

DFT calculation was further used to analyze the interaction of $S_2O_8^{2-}$ with different sites. Figure 11 simulates the adsorption of $S_2O_8^{2-}$ on modified gasification slags with different ratios of graphitic N to the carbonyl group, as well as the derivations of various functional groups and the distribution of carbonyl groups in the new theoretical model. The adsorption energy and transfer charge of the different ratios of graphitic N to a carbonyl group are shown in Table 7. All adsorption energies are negative, which means that the adsorption of PS is spontaneous. The adsorption energy of PS (E_{ads}) was defined as follows:

$$E_{ads} = E_{total} - E_{subs} - E_{PS} \quad (4)$$

The E_{total}, E_{subs}, and E_{PS} were defined as the energy of catalysts with PS, catalysts, and free PS, respectively. It was found that the model with a higher ratio of graphitic N to carbonyl group had the higher adsorption energy for $S_2O_8^{2-}$. A higher adsorption energy means a stronger interaction between the catalyst and PS. The results of the transfer charge verified that the electron transfer occurred between PS and the catalyst and that CGS-N_3 had the largest transfer charge. The above results further indicate that catalysts with higher graphitic N and carbonyl are more conducive to PS activation, which is consistent with the trend of TOF values.

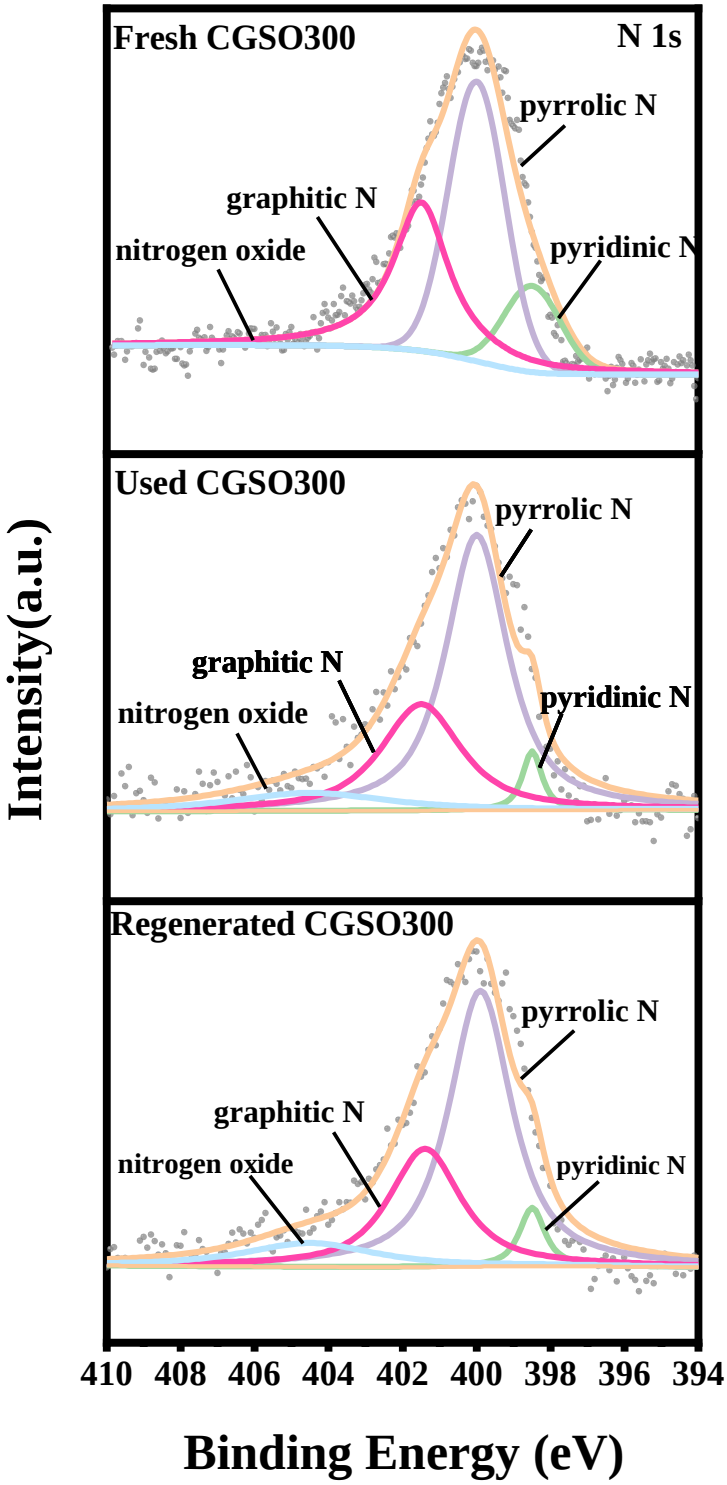

Figure 10. N 1s spectra of Fresh CGSO300, Used CGSO300, and Regenerated CGSO300.

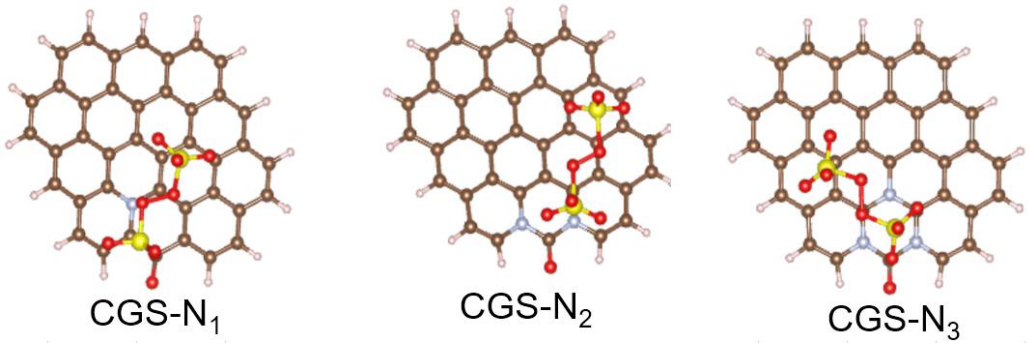

Figure 11. Structure of $S_2O_8^{2-}$ adsorbed on different sites.

Table 7. Adsorption energy and the transferred charge of different N-doped CGSs.

Catalysts	Ratio of Graphitic N to Carbonyl Group	Adsorption Energy (Ea, eV)	Transfer Charge (Q, e)
CGS-N_1	1:1	−1.982	−1.330
CGS-N_2	2:1	−2.979	−1.027
CGS-N_3	3:1	−3.870	−1.638

3. Experimental Procedure

3.1. Materials and Reagents

CGS was provided by Shaanxi Future Energy Chemical Co. (Yulin, China), methanol was supplied by Tianjin Tianli Chemical Reagent Co. (Tianjin, China), nitric acid (HNO_3) was provided by Tianjin Zhiyuan Chemical Reagent Co., Ltd. (Tianjin, China), and 4-acetaminophen (APAP, 99.0%) and potassium persulfate ($K_2S_2O_8$, 99.0%) were supplied by Macklin (Shanghai, China) and Aladdin (Shanghai, China). Ultrapure water was employed throughout the experiments.

3.2. Preparation of Modified Gasification Slag

During the nitric acid oxidation treatment, CGS was soaked in nitric acid (34%) at room temperature for 2 h. After filtering and washing to a neutral pH, the samples were dried in an oven at 80 °C to a constant weight, and then placed in a dryer for use, labeled as CGSO. The CGSO was placed in a quartz tube, calcined in N_2 at 300 °C for 1 h, and labeled as CGSO300.

3.3. Catalyst Characterization Methods

A Raman spectrometer (LabRAM HR800, Horiba, NJ, USA) with a 532 nm argon ion laser was used to detect the molecular structure of the material. The composition and chemical states of the elements on the surface of the carbon catalysts were determined by X-ray photoelectron spectroscopy (XPS, AXIS ULTRA DLD, Kratos, Manchester, UK) under irradiation with Al Kα X-ray (hv = 1486.6 eV). The textural properties of the gasification slag were determined using nitrogen sorption isotherms at 77 K using a TriStar II 3020. All samples were degassed at 80 °C for 8 h under vacuum before measurement. The specific surface area of the gasification slag adopted the Brunauer–Emmett–Teller (BET) method. The Barrett–Joyner–Halenda (BJH) calculation model for microporous carbon was used to measure the micropore surface area and volume of the samples. The pore volume and pore size distribution were determined from the volume adsorbed at a relative pressure of 0.99 and by using Density Functional Theory (DFT), respectively.

3.4. Measurement of Catalytic Activity

In this study, CGS, CGSO, and CGSO300 catalysts were used to activate persulfate for the catalytic degradation of acetaminophen. Firstly, 100 mL of acetaminophen solution (50 mgL^{-1}) with persulfate (2.5 mM) was continuously shanked in a thermostatic shaker. Then, 100 mgL^{-1} of CGS was added to the system. The reaction was initiated by adding

the catalyst to the solution. Following this, 1 mL of the solution was withdrawn at regular intervals and filtered through a 0.45 μm aqueous needle filter. The concentration of acetaminophen was analyzed by high-performance liquid chromatography (UHPLC, UltiMate3000, Dionex, Waltham, MA, USA) with a diode array detector (DAD) at λ = 280 nm. The chromatographic column was a SunFire™ C18 (4.6 × 150 mm, 5.0 μm) and the mobile phase was 30% methanol and 70% ultrapure water with a flow rate of 0.8 mLmin^{-1}. The column temperature was set as 30 °C.

3.5. Theoretical Calculation

Spin polarization density functional theory (DFT) was calculated based on plane waves using the Vienna ab simulation package [42]. All calculations were performed using generalized gradient approximation (GGA) with the Perdew–Burke–Ernzerhof (PBE) exchange-correlation function [43]. The Bader charge analysis method was applied to calculate charge transfers [44].

4. Conclusions

In this work, modified gasification slag was successfully synthesized for use as an activator for PS in the APAP degradation process. The catalytic activity of the modified gasification slag was enhanced by O/N doping combined with calcination. It was found that GCSO calcinated at 300 °C had the highest catalytic activity for PS activation, with 100% APAP removal in 30 min. O/N doping accelerated the electron transfer process, in which carbonyl and graphitic N were demonstrated to be the main active sites. We reported that the increase in carbonyl and graphitic N not only enhanced the catalytic performance towards PS activation but also effectively facilitated the nonradical pathway. The contributions of nonradical pathways on APAP degradation in the CGS/PS, CGSO/PS, and CGSO300/PS systems were calculated as 74%, 99%, and 100%, respectively. This results in the high anti-interference potential of the PS activation system by CGS. It was also found that a higher ratio of graphitic N to carbonyl group led to the higher catalytic activity of the modified gasification slag, which was also proven through the DFT calculation of the adsorption energy for $S_2O_8^{2-}$. This study provided a new feasible way for the degradation of organic pollutants using modified gasification slag to activate persulfate. Benefiting from its simple preparation process, modified gasification slag is anticipated to be a novel and cheap carbon catalyst for wastewater treatment.

Author Contributions: Investigation, W.S. and Y.N.; writing—original draft, W.S.; methodology, F.Q.; project administration, Z.Z.; software, Q.W.; writing—review and editing, F.Q., Z.Z. and Z.H.; supervision, K.W. and Z.H.; resources, Z.H. All authors have read and agreed to the published version of the manuscript.

Funding: This research was funded by the Fundamental Research Program of Shanxi Province (202103021224443), ICC CAS (SCJC-WRW-2022-19), the Youth Innovation Promotion Association of the Chinese Academy of Sciences (2022174, Z.Z.Q.), the Science and Technology Major Project of Shanxi Province (202005D121002), and Yulin University and the Dalian National Laboratory for Clean Energy (Grant YLU-DNL, Fund 2021003).

Data Availability Statement: The data presented in this study are available in the article.

Conflicts of Interest: The authors declare no conflict of interest.

References

1. Santos, J.L.; Aparicio, I.; Alonso, E.; Callejón, M. Simultaneous determination of pharmaceutically active compounds in wastewater samples by solid phase extraction and high-performance liquid chromatography with diode array and fluorescence detectors. *Anal. Chim. Acta* **2005**, *550*, 116–122. [CrossRef]
2. Zhang, H.; Cao, B.; Liu, W.; Lin, K.; Feng, J. Oxidative removal of acetaminophen using zero-valent aluminum-acid system: Efficacy, influencing factors, and reaction mechanism. *J. Environ. Sci.* **2012**, *24*, 314–319. [CrossRef]
3. Do, Q.C.; Kim, D.G.; Ko, S.O. Nonsacrificial Template Synthesis of Magnetic-Based Yolk-Shell Nanostructures for the Removal of Acetaminophen in Fenton-like Systems. *ACS Appl. Mater. Interfaces* **2017**, *9*, 28508–28518. [CrossRef]

4. Lu, H.; Zhu, Z.; Zhang, H.; Zhu, J.; Qiu, Y.; Zhu, L.; Kuppers, S. Fenton-Like Catalysis and Oxidation/Adsorption Performances of Acetaminophen and Arsenic Pollutants in Water on a Multimetal Cu-Zn-Fe-LDH. *ACS Appl. Mater. Interfaces* **2016**, *8*, 25343–25352. [CrossRef]
5. Basha, S.; Keane, D.; Nolan, K.; Oelgemoller, M.; Lawler, J.; Tobin, J.M.; Morrissey, A. UV-induced photocatalytic degradation of aqueous acetaminophen: The role of adsorption and reaction kinetics. *Environ. Sci. Pollut. Res. Int.* **2015**, *22*, 219–230. [CrossRef]
6. Jallouli, N.; Elghniji, K.; Trabelsi, H.; Ksibi, M. Photocatalytic degradation of paracetamol on TiO_2 nanoparticles and TiO_2/cellulosic fiber under UV and sunlight irradiation. *Arab. J. Chem.* **2017**, *10*, S3640–S3645. [CrossRef]
7. Ding, Y.; Fu, L.; Peng, X.; Lei, M.; Wang, C.; Jiang, J. Copper catalysts for radical and nonradical persulfate based advanced oxidation processes: Certainties and uncertainties. *Chem. Eng. J.* **2022**, *427*, 131776. [CrossRef]
8. Wen, Q.; Wang, Y.; Zeng, Z.; Qi, F.; Gao, P.; Huang, Z. Covalent organic frameworks-derived hierarchically porous N-doped carbon for 2,4-dichlorophenol degradation by activated persulfate: The dual role of graphitic N. *J. Hazard. Mater.* **2022**, *426*, 128065. [CrossRef]
9. Tian, K.; Shi, F.; Cao, M.; Zheng, Q.; Zhang, G. A Review of Persulfate Activation by Magnetic Catalysts to Degrade Organic Contaminants: Mechanisms and Applications. *Catalysts* **2022**, *12*, 1058. [CrossRef]
10. Gao, Y.; Wang, Q.; Ji, G.; Li, A. Degradation of antibiotic pollutants by persulfate activated with various carbon materials. *Chem. Eng. J.* **2022**, *429*, 132387. [CrossRef]
11. Xie, X.; Liu, Y.; Li, Y.; Tao, J.; Liu, C.; Feng, J.; Feng, L.; Shan, Y.; Yang, S.; Xu, K. Nitrogen-doped Fe-MOFs derived carbon as PMS activator for efficient degradation of tetracycline. *J. Taiwan Inst. Chem. Eng.* **2023**, *146*, 104891. [CrossRef]
12. Wu, L.; Wu, T.; Liu, Z.; Tang, W.; Xiao, S.; Shao, B.; Liang, Q.; He, Q.; Pan, Y.; Zhao, C.; et al. Carbon nanotube-based materials for persulfate activation to degrade organic contaminants: Properties, mechanisms and modification insights. *J. Hazard. Mater.* **2022**, *431*, 128536. [CrossRef]
13. Luo, J.; Yi, Y.; Fang, Z. Nitrogen-rich magnetic biochar prepared by urea was used as an efficient catalyst to activate persulfate to degrade organic pollutants. *Chemosphere* **2023**, *339*, 139614. [CrossRef]
14. Qi, F.; Zeng, Z.; Wen, Q.; Huang, Z.; Wang, Y.; Xu, Y. Asymmetric enhancement of persulfate activation by N-doped carbon microelectrode: Electro-adsorption and activation pathway regulation. *Sep. Purif. Technol.* **2022**, *301*, 121916. [CrossRef]
15. Xu, J.; Zhou, P.; Shi, P.; Min, Y.; Xu, Q. Insights into the multiple mechanisms of chlorophenols oxidation via activating peroxymonosulfate by 3D N-doped porous carbon. *J. Environ. Chem. Eng.* **2021**, *9*, 106545. [CrossRef]
16. Manz, K.E.; Kulaots, I.; Greenley, C.A.; Landry, P.J.; Lakshmi, K.V.; Woodcock, M.J.; Hellerich, L.; Bryant, J.D.; Apfelbaum, M.; Pennell, K.D. Low-temperature persulfate activation by powdered activated carbon for simultaneous destruction of perfluorinated carboxylic acids and 1,4-dioxane. *J. Hazard. Mater.* **2023**, *442*, 129966. [CrossRef]
17. Yu, W.; Zhang, H.; Wang, X.; Rahman, Z.U.; Shi, Z.; Bai, Y.; Wang, G.; Chen, Y.; Wang, J.; Liu, L. Enrichment of residual carbon from coal gasification fine slag by spiral separator. *J. Environ. Manag.* **2022**, *315*, 115149. [CrossRef]
18. Liu, X.; Jin, Z.; Jing, Y.; Fan, P.; Qi, Z.; Bao, W.; Wang, J.; Yan, X.; Lv, P.; Dong, L. Review of the characteristics and graded utilization of coal gasification slag. *Chin. J. Chem. Eng.* **2021**, *35*, 92–106. [CrossRef]
19. Ren, L.; Ding, L.; Guo, Q.; Gong, Y.; Yu, G.; Wang, F. Characterization, carbon-ash separation, and resource utilization of coal gasification fine slag: A comprehensive review. *J. Clean. Prod.* **2023**, *398*, 136554. [CrossRef]
20. Yuan, N.; Zhao, A.; Hu, Z.; Tan, K.; Zhang, J. Preparation and application of porous materials from coal gasification slag for wastewater treatment: A review. *Chemosphere* **2022**, *287 Pt 2*, 132227. [CrossRef]
21. Li, X.; Liu, X.; Huang, X.; Lin, C.; He, M.; Ouyang, W. Activation of peroxymonosulfate by WTRs-based iron-carbon composites for atrazine removal: Performance evaluation, mechanism insight, and byproduct analysis. *Chem. Eng. J.* **2021**, *421*, 127811. [CrossRef]
22. Long, Y.; Yang, P.; Wang, C.; Wu, W.; Chen, X.; Liu, W.; Cao, Z.; Zhan, X.; Liu, D.; Huang, W. Peroxymonosulfate activation by iron-carbon composite derived from coal gasification slag for sulfamethoxazole removal: Performance evaluation and mechanism insight. *Chem. Eng. J.* **2023**, *456*, 140996. [CrossRef]
23. Liu, B.; Lv, P.; Wu, R.; Bai, Y.; Wang, J.; Su, W.; Song, X.; Yu, G. Coal gasification fine slag based multifunctional nanoporous silica microspheres for synergistic adsorption of Pb(II) and Congo red. *Sep. Purif. Technol.* **2023**, *323*, 124478. [CrossRef]
24. Palaniselvam, T.; Aiyappa, H.B.; Kurungot, S. An efficient oxygen reduction electrocatalyst from graphene by simultaneously generating pores and nitrogen-doped active sites. *J. Mater. Chem.* **2012**, *22*, 23799–23805. [CrossRef]
25. Dresselhaus, M.S.; Jorio, A.; Hofmann, M.; Dresselhaus, G.; Saito, R. Perspectives on carbon nanotubes and graphene Raman spectroscopy. *Nano Lett.* **2010**, *10*, 751–758. [CrossRef]
26. Demiral, İ.; Samdan, C.; Demiral, H. Enrichment of the surface functional groups of activated carbon by modification method. *Surf. Interfaces* **2021**, *22*, 100873. [CrossRef]
27. He, H.; Jiang, B.; Yuan, J.; Liu, Y.; Bi, X.; Xin, S. Cost-effective electro generation of H_2O_2 utilizing HNO_3 modified graphite/polytetrafluoroethylene cathode with exterior hydrophobic film. *J. Colloid Interface Sci.* **2019**, *533*, 471–480. [CrossRef]
28. Wang, X.; Zhu, W.; Wang, N.; Zuo, X. Nitrogen-doped oxidized activated carbon as efficient metal-free bifunctional material for bisphenol removal: A tuning of surface chemistry. *J. Environ. Chem. Eng.* **2022**, *10*, 108509. [CrossRef]
29. Forouzesh, M.; Ebadi, A.; Aghaeinejad-Meybodi, A.; Khoshbouy, R. Transformation of persulfate to free sulfate radical over granular activated carbon: Effect of acidic oxygen functional groups. *Chem. Eng. J.* **2019**, *374*, 965–974. [CrossRef]

30. Yang, W.; Jiang, Z.; Hu, X.; Li, X.; Wang, H.; Xiao, R. Enhanced activation of persulfate by nitric acid/annealing modified multi-walled carbon nanotubes via non-radical process. *Chemosphere* **2019**, *220*, 514–522. [CrossRef]
31. Duan, X.; Ao, Z.; Sun, H.; Indrawirawan, S.; Wang, Y.; Kang, J.; Liang, F.; Zhu, Z.H.; Wang, S. Nitrogen-doped graphene for generation and evolution of reactive radicals by metal-free catalysis. *ACS Appl. Mater. Interfaces* **2015**, *7*, 4169–4178. [CrossRef]
32. Gao, Y.; Zhu, Y.; Lyu, L.; Zeng, Q.; Xing, X.; Hu, C. Electronic Structure Modulation of Graphitic Carbon Nitride by Oxygen Doping for Enhanced Catalytic Degradation of Organic Pollutants through Peroxymonosulfate Activation. *Environ. Sci. Technol.* **2018**, *52*, 14371–14380. [CrossRef]
33. Li, H.; Li, N.; Zuo, P.; Qu, S.; Shen, W. Efficient adsorption-reduction synergistic effects of sulfur, nitrogen and oxygen heteroatom co-doped porous carbon spheres for chromium(VI) removal. *Colloids Surf. A Physicochem. Eng. Asp.* **2021**, *618*, 126502. [CrossRef]
34. Meng, Y.; Li, Z.; Tan, J.; Li, J.; Wu, J.; Zhang, T.; Wang, X. Oxygen-doped porous graphitic carbon nitride in photocatalytic peroxymonosulfate activation for enhanced carbamazepine removal: Performance, influence factors and mechanisms. *Chem. Eng. J.* **2022**, *429*, 130860. [CrossRef]
35. Pham, X.N.; Nguyen, H.T.; Pham, T.N.; Nguyen, T.T.-B.; Nguyen, M.B.; Tran, V.T.-T.; Doan, H.V. Green synthesis of H-ZSM-5 zeolite-anchored O-doped g–C_3N_4 for photodegradation of Reactive Red 195 (RR 195) under solar light. *J. Taiwan Inst. Chem. Eng.* **2020**, *114*, 91–102. [CrossRef]
36. Alvandi, M.; Nourmoradi, H.; Nikoonahad, A.; Aghayani, E.; Abbas Mirzaee, S. LED visible light assisted photo-oxidation of acetaminophen using *a* one-step synthesis of Cu, Fe@g-C_3N_4 nanosheet—Activated persulfate system in aqueous solutions. *Arab. J. Chem.* **2023**, *16*, 105251. [CrossRef]
37. An, S.; Zhang, G.; Wang, T.; Zhang, W.; Li, K.; Song, C.; Miller, J.T.; Miao, S.; Wang, J.; Guo, X. High-Density Ultra-small Clusters and Single-Atom Fe Sites Embedded in Graphitic Carbon Nitride (g-C_3N_4) for Highly Efficient Catalytic Advanced Oxidation Processes. *ACS Nano* **2018**, *12*, 9441–9450. [CrossRef]
38. Li, W.; Nie, C.; Wang, X.; Ye, H.; Li, D.; Ao, Z. Alkaline lignin-derived N-doped biochars as peroxymonosulfate activators for acetaminophen degradation: Performance and catalytic bridging mediated Electron-Transfer mechanism. *Sep. Purif. Technol.* **2023**, *323*, 124418. [CrossRef]
39. Tan, C.; Gao, N.; Deng, Y.; Deng, J.; Zhou, S.; Li, J.; Xin, X. Radical induced degradation of acetaminophen with Fe_3O_4 magnetic nanoparticles as *a* heterogeneous activator of peroxymonosulfate. *J. Hazard. Mater.* **2014**, *276*, 452–460. [CrossRef]
40. Zhang, Y.; Zhang, Q.; Dong, Z.; Wu, L.; Hong, J. Structurally modified $CuFe_2O_4$/persulfate process for acetaminophen scavenging: High efficiency with low catalyst addition. *J. Chem. Technol. Biotechnol.* **2018**, *94*, 785–794. [CrossRef]
41. Zhu, Z.; Zhang, Q.; Xu, M.; Xue, Y.; Zhang, T.; Hong, J. Highly active heterogeneous FeCo metallic oxides for peroxymonosulfate activation: The mechanism of oxygen vacancy enhancement. *J. Environ. Chem. Eng.* **2023**, *11*, 109071. [CrossRef]
42. Morales-Garcia, A.; Rhatigan, S.; Nolan, M.; Illas, F. On the use of DFT+U to describe the electronic structure of TiO_2 nanoparticles: $(TiO_2)35$ as a case study. *J. Chem. Phys.* **2020**, *152*, 244107. [CrossRef]
43. Samat, M.H.; Ali AM, M.; Taib MF, M.; Hassan, O.H.; Yahya, M.Z.A. Structural and electronic properties of TiO_2 polymorphs with effective on-site coulomb repulsion term: DFT+U approaches. *Mater. Today Proc.* **2019**, *17*, 472–483. [CrossRef]
44. Qi, F.; Wang, Q.; Zeng, Z.; Wen, Q.; Huang, Z. Insight into the roles of microenvironment and active site on the mechanism regulation in metal-free persulfate activation process coupling with an electric field. *J. Hazard. Mater.* **2022**, *439*, 129673. [CrossRef]